

Accepted Manuscript

Research paper

CuO-decorated dual-phase TiO₂ microspheres with enhanced activity for photocatalytic CO₂ reduction in liquid–solid regime

Yunxia Zhao, Jiabin Chen, Wei Cai, Yunfei Bu, Qiong Huang, Tao Tao, Jiangang Lu

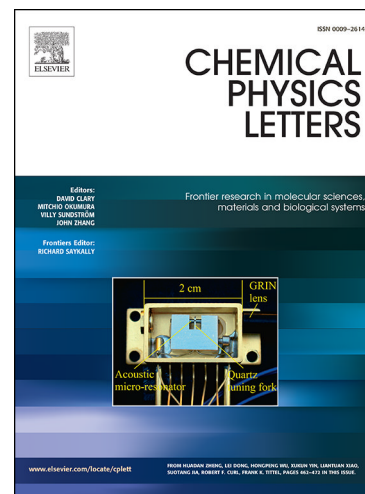
PII: S0009-2614(19)30281-7
DOI: <https://doi.org/10.1016/j.cplett.2019.04.010>
Reference: CPLETT 36364

To appear in: *Chemical Physics Letters*

Received Date: 27 December 2018
Revised Date: 2 April 2019
Accepted Date: 4 April 2019

Please cite this article as: Y. Zhao, J. Chen, W. Cai, Y. Bu, Q. Huang, T. Tao, J. Lu, CuO-decorated dual-phase TiO₂ microspheres with enhanced activity for photocatalytic CO₂ reduction in liquid–solid regime, *Chemical Physics Letters* (2019), doi: <https://doi.org/10.1016/j.cplett.2019.04.010>

This is a PDF file of an unedited manuscript that has been accepted for publication. As a service to our customers we are providing this early version of the manuscript. The manuscript will undergo copyediting, typesetting, and review of the resulting proof before it is published in its final form. Please note that during the production process errors may be discovered which could affect the content, and all legal disclaimers that apply to the journal pertain.



CuO-decorated dual-phase TiO₂ microspheres with enhanced activity for photocatalytic CO₂ reduction in liquid–solid regime

Yunxia Zhao, Jiabin Chen, Wei Cai^{*}, Yunfei Bu, Qiong Huang, Tao Tao, Jiangang Lu

Jiangsu Collaborative Innovation Center of Atmospheric Environment & Equipment Technology, Jiangsu Key Laboratory of Atmospheric Environment Monitoring and Pollution Control, School of Environmental Science and Engineering, Nanjing University of Information Science & Technology, Nanjing 210044, PR China.

Abstract

Copper oxide (CuO)-decorated anatase and TiO₂(B) dual-phase titania microsphere (CuO/TiO₂(AB)) photocatalysts were synthesized using a facile two-step approach. The photocatalytic reduction of CO₂ to form methyl formate (MF) in methanol was evaluated. The results indicated that the CuO-decorated dual-phase TiO₂ microspheres displayed MF yield of 1800 $\mu\text{mol}\cdot\text{g}^{-1}$ under 4 h illumination, higher than other reference photocatalysts, due to its mixed-phase heterojunction structure and larger surface area, thus leading to an enhanced UV-light response, effective separation and low recombination rate of the photoinduced charge carriers. CuO/TiO₂(AB) also showed good stability with the MF yield reproducibility greater than 90% in cyclic runs.

Keywords: Photocatalytic CO₂ reduction, Anatase TiO₂, TiO₂ (B), CuO loading, Heterojunctions

1. Introduction

*Corresponding author

E-mail: caiwei_19880105@163.com; Tel: +86 25 58731090

Carbon dioxide (CO₂) is a carbon source that possesses a very high energy potential and could serve as a sustainable energy source. The photocatalytic conversion of waste CO₂ into energy-rich hydrocarbon fuels or more valuable chemicals is a promising method to address two major problems: the imminent energy crisis and anthropogenic climate change. Titanium dioxide (TiO₂), the earliest studied photocatalyst^[1], has advantages such as being nontoxic, lossless and environmentally friendly. Among the many well-studied photocatalysts, TiO₂ has attracted much attention and has been the focus of research due to its high activity, high thermal stability, durability, low cost, nontoxicity and other characteristics.^[2] However, as a single-component semiconductor photocatalyst, TiO₂ has an inherent drawback, i.e., its rapid photogenerated electron/hole (e⁻/h⁺) pair recombination (~10 ns); hence, only a fraction of the generated e⁻/h⁺ pairs are available for photoreaction^[3,4]. To further improve the photocatalytic performance of TiO₂, numerous methods, including metal/nonmetal doping, metal loading, heterojunction construction and coupling with carbon materials, have been proposed^[5]. Jiang et al.^[6] assembled a TiO₂/active carbon-Ag ternary composite photocatalyst for the photocatalytic conversion of CO₂ using H₂O as the reducing agent. The composite photocatalyst exhibited a six-fold increase in the CO yield compared to that obtained with pristine TiO₂. Li et al.^[7] reported a promising N-rich carbon quantum dot/TiO₂ photocatalyst for CO₂ photoreduction by gaseous water under simulated solar irradiation. As a result, 1.838 μmol CO and 1.195 μmol CH₄ were obtained from CO₂ reduction on 50 mg of photocatalyst after 6 h of irradiation. Zhao et al.^[8] synthesized a graphene-wrapped Pt/TiO₂ photocatalyst with high photocatalytic activity and selectivity for CO₂ conversion; the formation rate of CH₄ was 41.3 μmol·g⁻¹·h⁻¹, and the selectivity of the CO₂ conversion to CH₄ was 99.1%.

All of the above co-catalysts can extend the light absorption range and suppress the recombination and transfer of charge carriers, resulting in superior CO₂ photoconversion performance. However, the limited reserves, inaccessibility and high cost of these co-catalysts, often due to the use of noble metals, limit their practical applications. As an alternative, the incorporation of CuO into TiO₂ is a less expensive option^[9-12]. CuO has a band gap of 1.6 eV that, in principle, should favour the absorption of visible light and improve the photocatalytic activity. Gao et al.^[13] designed an innovative noble metal-free inorganic nanocomposite (hollow TiO₂/CuO) that is capable of displaying both photochromism and catalysis effects under solar irradiation. Taufik et al.^[14] successfully synthesized ternary CuO/TiO₂/ZnO nanocomposites to investigate their photocatalytic degradation of methylene blue. Under optimal conditions, 100% and 98% of the methylene blue was removed within 2 h under UV and visible light, respectively. The results showed that holes were the main active species in the degradation process. Razali et al.^[15] reported that CuO-loaded TiO₂ nanotube photocatalysts demonstrated a higher CO₂ conversion efficiency than TiO₂ nanotubes because the former could effectively separate photogenerated electron-hole pairs due to the presence of CuO.

Given the above, CuO can serve as an effective co-catalyst for CO₂ photoreduction. The main catalyst, TiO₂, has at least 11 different phases.^[16] The most well-known phases are anatase, rutile, and brookite. Anatase is the most investigated allotrope due to its relatively high photocatalytic activity. TiO₂(B) is another polymorph of TiO₂ and possesses a more negative conduction band (CB) edge than anatase^[17]. To date, polyphase TiO₂^[7] has rarely been studied for photocatalytic CO₂ reduction. By the definition of a heterojunction, the interface between two different phases with unequal band structures can enhance the optical adsorption of photocatalysts. Si et al.^[18]

prepared a novel composite with anatase TiO₂ quantum dots grown on TiO₂ (B) nanosheets for photocatalytic H₂ production, which showed a high photocatalytic activity, approximately 45 times higher than that of rutile-anatase mixed Degussa P25. The anatase and B mixed phase promoted efficient charge separation at the interface, while a relatively high conduction band edge of TiO₂ (B) with respect to the redox potential level of H⁺/H₂ leads to a further enhancement of the photocatalytic activity.

In this paper, CuO-decorated anatase and TiO₂ (B) dual-phase titania microspheres were prepared for the photocatalytic conversion of CO₂ by methanol. To the best of our knowledge, there has been no report on this catalyst for CO₂ photoreduction. Three other materials, namely, pure anatase TiO₂, CuO-loaded anatase TiO₂ and anatase-B polyphase TiO₂, were compared with the objective catalyst to highlight its unique synergistic advantage of mixed phases and CuO loading. The optical catalysis reaction system was a catalyst-methanol slurry regime at room temperature and atmospheric pressure. Methanol was used as a reducing agent because it has a higher CO₂ absorption capacity than H₂O. Meanwhile it was a sacrificial agent to avoid introducing other toxic sacrificial agent such as acetonitrile. Improving the CO₂ absorption capacity, extending the light absorption range and intensity and suppressing carrier recombination are expected to enhance the efficiency for the photocatalytic conversion of CO₂.

2. Experimental Section

2.1. Photocatalyst preparation

First, single-component anatase TiO₂, referred to as TiO₂(A), was synthesized by a sol-gel process^[19-21]. A total of 10 g tetrabutyltitanate was dissolved in 10 mL ethanol by vigorous stirring for 30 min, and 1.3 g CTAB was dissolved in 10 mL ethanol using the ultrasonic

dissolution method. Then, the above two solutions were mixed together and stirred for 30 min. After ageing for 12 h at room temperature, a sol formed. The sol was dried at 100 °C for 12 h and then calcined at 450 °C for 6 h with a heating rate of 2 °C/min.

The anatase and B dual-phase TiO₂ were synthesized by the solvothermal method^[22]. Tetrabutyltitanate (0.1 mL) was added to 10 mL acetic acid and vigorously stirred for 10 min at room temperature. Then, the solution was transferred into a 100-mL Teflon-lined stainless-steel autoclave and maintained at 180 °C for 12 h. The reaction vessel was cooled naturally to room temperature, and then the precipitate was collected by suction filtration. After washing repeatedly with ethanol and drying at 80 °C overnight, the powder was calcined at 370 °C for 2 h and named TiO₂(AB).

CuO-incorporated TiO₂ composites were prepared using an impregnation method. They were named CuO-TiO₂(A) and CuO/TiO₂(AB). Taking CuO/TiO₂(AB) as an example, 0.1 g of as-prepared TiO₂(AB) was added into a certain concentration solution of Cu(NO₃)₂. A homogeneous phase system was made by ultrasonic dispersion technology. Then, the above suspension was dried in a constant-temperature bath followed by further drying at 120 °C for 12 h in an electric oven. The final product was obtained by calcination in a muffle furnace at 400 °C with a heating rate of 1 °C•min⁻¹ for 2 h.

2.2. Photocatalyst characterization

X-ray powder diffraction (XRD) analysis was carried out using a Philips X'Pert Pro XRD instrument with Cu K α X-ray radiation. The Raman spectra were recorded using a RENISHAW spectrometer with an excitation laser of 532 nm. Scanning electron microscopy (SEM) was performed using a Hitachi S4800 microscope. Before the test, the samples were treated by gold

coating. High-resolution transmission electron microscopy (HR-TEM) studies were performed on a JEM-2100 (JEOL, Japan) instrument equipped with a slow-scan CCD camera and an accelerating voltage of 200 kV. N₂ adsorption-desorption isotherms were measured at -196 °C using a Micromeritics ASAP 2020 physisorption instrument. The surface areas and porosity were obtained by Brunauer-Emmett-Teller (BET) and Barrett-Joyner-Halender (BJH) method. X-ray photoelectron spectroscopy (XPS) analyses were performed on an ESCALAB 250 spectrometer (Thermo, U.S.A.). All binding energies (BE) were referenced to the adventitious C1s at 284.4 eV [23, 24]. The X-ray source utilized was Al K α X-ray (hv=1486.6 eV) radiation. Ultraviolet-visible diffuse reflectance spectroscopy (DRS) was performed on a Shimadzu UV-2600 spectrometer. Photoluminescence (PL) spectra were recorded on a Hitachi F-4500 instrument with an excitation wavelength of 325 nm at room temperature. Electrochemical impedance spectroscopy (EIS) measurements and the photocurrents were obtained using a CHI760 electrochemical working station with a standard three-electrode system and 0.5 mol·L⁻¹ Na₂SO₄ as the electrolyte solution. FTO glass was dip-coated with a mixed solution of the photocatalyst, naphthol, deionized water and alcohol and used as the work electrode.

2.3. Photocatalytic activity tests

The photocatalytic efficiency of the obtained samples was evaluated by the production of HCOOCH₃ using a 50 mL quartz tube as a photocatalytic reactor. A 250-W Hg lamp (BL-GHX-V, Shanghai BiLon, China) was positioned parallel to and 15 cm away from one side of the photocatalytic reactor as a light source. The irradiation intensity was measured about 3900 $\mu\text{W}/\text{cm}^2$ at 365 nm which is the main radiation wavelength of the lamp. Typically, 30 mg of the photocatalyst was added into a pure CH₃OH solution (30 mL), and pure CO₂ gas was then injected

into the closed reaction system for 30 min. Before the light irradiation, the solution was saturated with CO₂ gas to ensure that an adsorption-desorption equilibrium was achieved. The magnetic stirrer at the bottom provided ideal mixing. The product from the photocatalytic reaction, HCOOCH₃, was analysed using gas chromatography (GC 9790 II, China) with a flame ionization detector.

3. Results and Discussion

3.1. Characterization of photocatalysts

3.1.1. Structural properties

The phase structures of these photocatalysts were investigated by XRD, as shown in Fig. 1 (i). The XRD patterns of TiO₂(A) and CuO-TiO₂(A) match well with that of anatase-phase TiO₂ (PDF# 21-1272) with diffraction peaks at 25.3°, 36.9°, 37.8°, 38.6°, 48.0°, 53.9°, 55.1°, 62.1°, 62.7°, 68.7°, 70.3°, 74.0°, 75.0° and 76.0° that can be indexed to the (101), (103), (004), (112), (200), (105), (211), (213), (204), (116), (220), (107), (215) and (301) crystal facets, respectively. The XRD patterns of TiO₂(AB) and CuO/TiO₂(AB) are similar to the standard spectrum of the monoclinic polymorph TiO₂(B) (PDF# 46-1237). However, a very obvious peak at 37.5° and a less obvious peak at 70.0° indicate that the TiO₂(AB) and CuO/TiO₂(AB) are not single-phase materials but contain some anatase phase. Based on the XRD patterns, TiO₂(A) and CuO-TiO₂(A) have a single phase, while TiO₂(AB) and CuO/TiO₂(AB) have two phases. CuO is not detected in the composites, which might be due to its low content and high dispersity. However, the intensities of the peaks increase with the incorporation of CuO, indicating the influence of CuO on the crystallization of TiO₂.

Figure 1 (ii) shows the Raman spectra of the prepared samples. As reported in the

literature^[8,18,25], the characteristic Raman peaks of the anatase phase are located at 395, 516, and 638 cm^{-1} and those of $\text{TiO}_2(\text{B})$ are located at 210, 256, 382, 422, 477, 553, 632, and 828 cm^{-1} ^[18]. For $\text{TiO}_2(\text{A})$ and $\text{CuO-TiO}_2(\text{A})$, only the Raman peaks corresponding to anatase TiO_2 can be detected, indicating the formation of a pure anatase phase. For $\text{TiO}_2(\text{AB})$ and $\text{CuO-TiO}_2(\text{AB})$, peak differentiation was used to confirm their phase formation due to undistinguishable peaks. The results show the presence of characteristic peaks for both anatase and $\text{TiO}_2(\text{B})$, implying that mixed phases are present. Based on the intensity of these peaks, the contributions of both phases are considerable. The XRD results are confirmed here, including the changes in the peak intensities after the CuO addition. Similarly, the Raman peaks of CuO are not detected in the composites of CuO and TiO_2 .

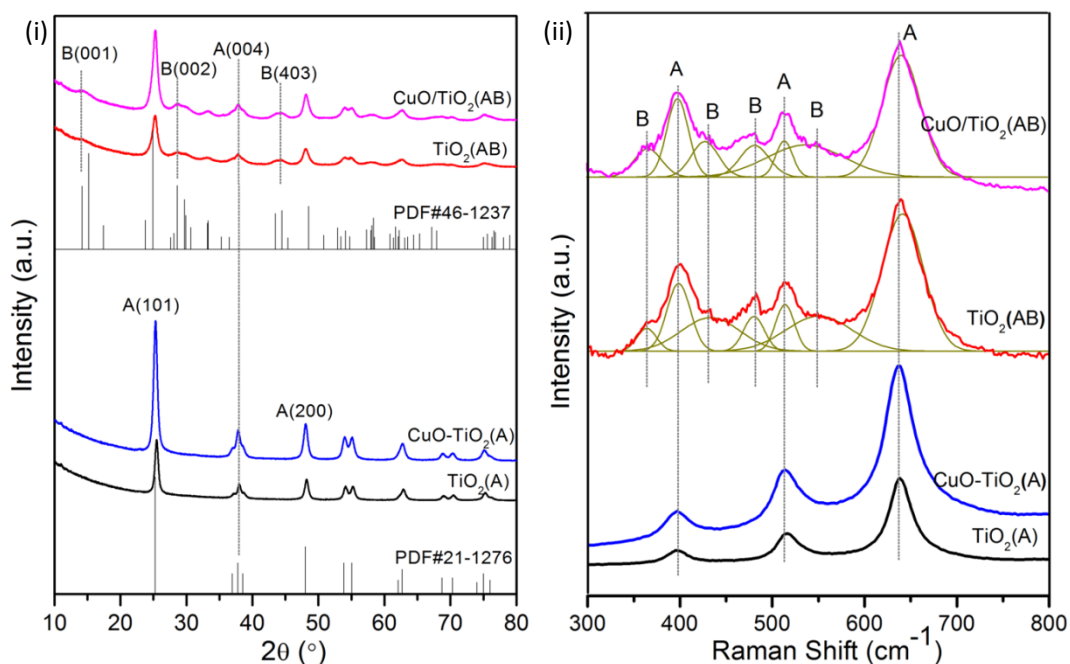


Fig. 1. (i) XRD patterns and (ii) Raman spectra of single-component TiO_2 and its composites with CuO . (A and B refer to the anatase and $\text{TiO}_2(\text{B})$ phases, respectively.)

The morphologies of the as-synthesized pure TiO_2 and CuO/TiO_2 composites were investigated by SEM, as shown in Fig. 2. The samples were not treated by grinding, ultrasound or other size reduction procedures before the test. The images show that $\text{TiO}_2(\text{A})$ and $\text{CuO-TiO}_2(\text{A})$

have anomalous bulk structures with non-uniform sizes and agglomerated nanoparticles. $\text{TiO}_2(\text{AB})$ and $\text{CuO}/\text{TiO}_2(\text{AB})$ have highly dispersed microsphere structures with diameters of $\sim 2 \mu\text{m}$. The microspheres are composed of numerous well-defined, smooth nanoplates with sharp edges. The acetic acid present in the reaction system could promote the formation of this hierarchical structure^[26]. The size of $\text{TiO}_2(\text{AB})$ is more evenly distributed than that of $\text{CuO}/\text{TiO}_2(\text{AB})$. In short, the dual-phase TiO_2 samples possess more order and better dispersal than the single-phase TiO_2 samples. Moreover, the smaller particle size is more beneficial to electron transfer^[27].

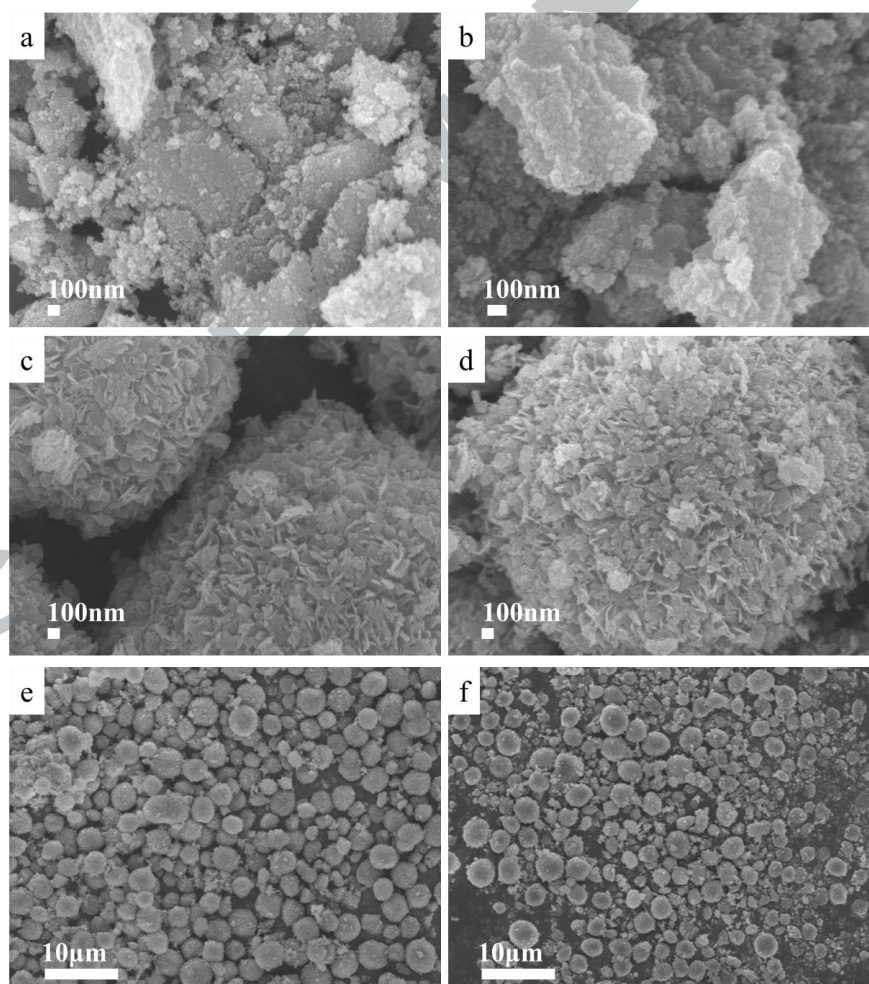


Fig. 2. SEM images of all the prepared samples. a) $\text{TiO}_2(\text{A})$, b) $\text{CuO-TiO}_2(\text{A})$, c, e) $\text{TiO}_2(\text{AB})$, and d, f) $\text{CuO}/\text{TiO}_2(\text{AB})$.

Figure 3a displays a TEM image of the $\text{CuO}/\text{TiO}_2(\text{AB})$ microspheres consisting of

aggregated nanosheets. The HRTEM image (Fig. 3b) shows lattice fringes with d spacings of 0.356, 0.352 and 0.233 nm. According to the XRD standard PDF cards, the former two spacings can be ascribed to the (110) plane of $\text{TiO}_2(\text{B})$ and (101) plane of anatase TiO_2 , respectively. The 0.233 nm spacing may correspond to the (111) plane of CuO or the (112) plane of anatase TiO_2 . This image cannot confirm the presence of crystalline CuO in the dual-phase TiO_2 composites. Therefore, further characterization is required to determine the overall chemical composition.

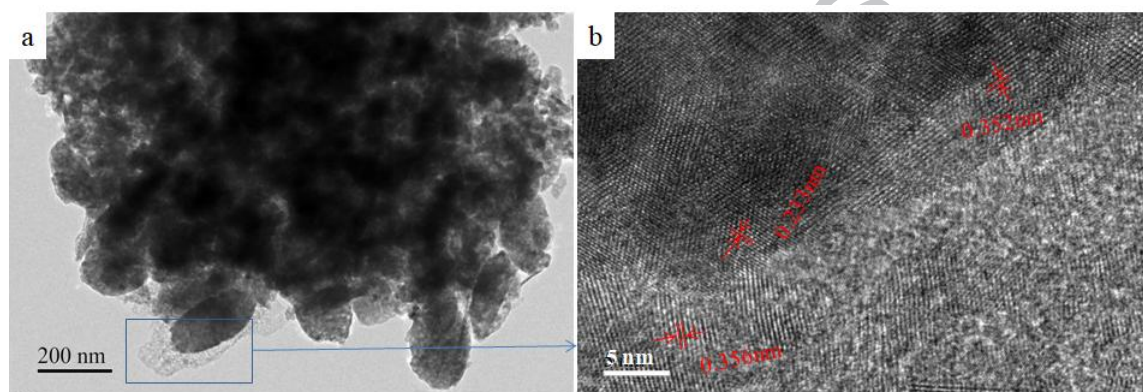


Fig. 3. (a) TEM and (b) HRTEM images of $\text{CuO}/\text{TiO}_2(\text{AB})$.

Fig. 4 presented the nitrogen sorption isotherms and BJH pore size distribution curves of the as-prepared samples. Their typical type IV isotherms with a distinct hysteresis loop are the characteristic feature of mesopores^[11,14]. The mixed-phase TiO_2 samples show a broad pore size distribution than the anatase samples, as indicated in Fig. 4(ii). The calculated BET surface area and pore volume of all these samples are summarized in Table S1. Obviously, the polyphase TiO_2 samples possess higher surface area and pore volume than the anatase samples due to smaller particle size and richer porosity.

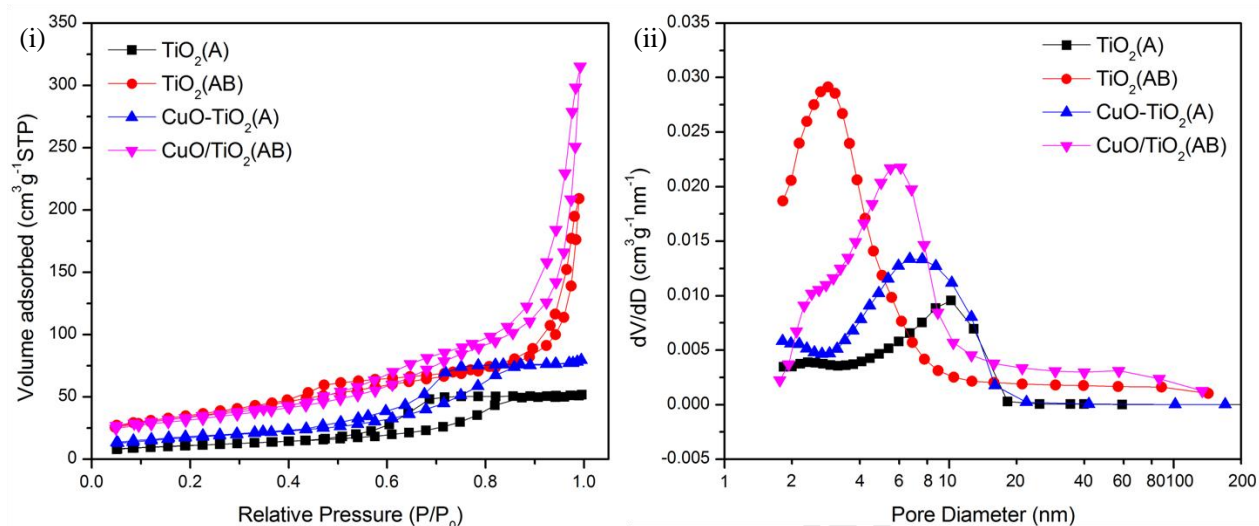


Fig. 4. (i) N₂ adsorption-desorption isotherms and (ii) BJH pore size distribution curves of single-component TiO₂ and its composites with CuO.

3.1.2. Chemical composition

Figure S1 shows the EDS and elemental mapping results for CuO/TiO₂(AB), confirming the presence of Ti, O, and Cu finely dispersed on the surface of the dual-phase TiO₂. Table S2 summarizes the weight percentages and atomic percentages of the above elements in CuO/TiO₂(AB). The Cu content in the composites is approximately 6 wt.%, and the atomic percent of O matches well with the atomic ratios of TiO₂ and CuO.

The surface chemical compositions and valence states of various elements in the synthesized materials were examined through XPS, as shown in Fig. 5. The survey scan spectra (Fig. 5 i) indicate the presence of C, O and Ti in the two TiO₂ samples and Cu in the TiO₂ and CuO composites. Among these elements, C is contamination, as explained in the experimental section.

Fig. 5ii displays the O 1s spectra; the spectra can be separated into two peaks at approximately 532.0 and 530.0 eV that can be assigned to O-H and Ti-O bonds, respectively, which are attributed to Ti-OH linkages and Ti-O-Ti (lattice O). As reported in the literature^[17, 18, 21], the bridging hydroxyl groups (Ti-O-H) are known to come from the dissociative adsorption of water on the TiO₂ surface. In Fig. 5ii, the intensity of this shoulder peak for CuO/TiO₂(AB) is higher than that

of the other three samples. The hydroxyl oxygen could capture electrons to produce active species ($\bullet\text{OH}$ and $\bullet\text{O}_2$), and these species would accelerate the photoreaction^[15]. The Ti 2p XPS spectra (Fig. 5iii) of all synthesized samples are almost the same; the Ti 2p_{1/2} and Ti 2p_{3/2} peaks are centred at binding energy values of 464.5 and 458.7 eV, respectively, which correspond to Ti^{4+} species^[17, 21]. The binding energies of Cu 2p_{3/2} and Cu 2p_{1/2} are 932.6-933.1 eV and 952.7-952.8 eV, respectively, for the two CuO-loaded composites (Fig. 5iv), suggesting that the existence of element Cu^[28]. Although the binding energy of CuO and Cu₂O is very close and difficult to distinguish, the absence of shake-up satellite peaks between the two Cu 2p peaks implies the presence of Cu₂O^[12], which disagrees with the results from EDS. It has been explained by that different chemical states of copper were caused by the sample being modified in the high vacuum environment of XPS and simultaneous exposure to X-rays^[12]. Thus, the Cu^{2+} translated into Cu^+ under the crucial working environment in XPS analysis. The binding energy of Cu 2p in CuO/TiO₂(AB) has a positive shift, which can be seen as evidence of the different chemical environments of Cu in the ternary system.

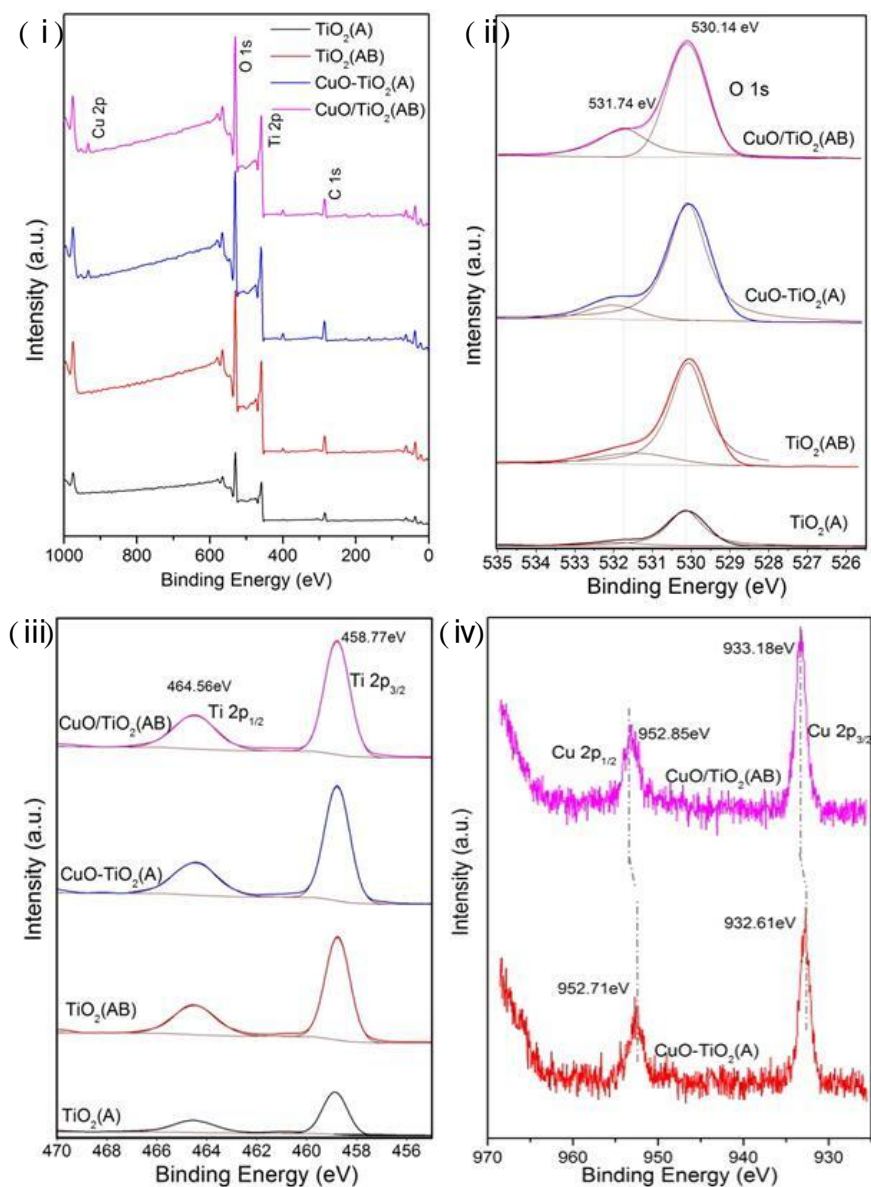


Fig. 5. (i) XPS survey spectra of the synthesized samples and high-resolution spectra of (ii) O 1s (iii) Ti 2p and (iv) Cu 2p.

3.1.3. Optical properties

The optical properties of the as-prepared photocatalysts were measured by UV-vis DRS, as shown in Fig. 6. As one can see in Fig. 6 i, after modification with CuO, the single-phase and dual-phase TiO₂ samples show enhanced light absorption in both the ultraviolet and visible-light ranges. A higher absorption intensity indicates a higher rate of electron-hole pair formation on the photocatalyst surface, resulting in the photocatalyst exhibiting a higher photocatalytic activity.

Compared to the single-phase samples, the UV-vis DRS spectra of the dual-phase samples shift to shorter wavelengths, which indicates that the incorporation of B phase TiO_2 into anatase TiO_2 increases the light absorption threshold. The adsorption wavelength is related to the band gap. As reported in the literature^[18], the conduction band (CB) level of B phase TiO_2 is higher than that of anatase TiO_2 . Based on the Kubelka-Munk function, the UV-vis spectra were converted into Tauc plots, as shown in Fig. 6 ii. The corresponding plots of $(\alpha h\nu)^2$ versus the photon energy ($h\nu$) can be used to determine the band gaps by extrapolating the maximum slope to the x axis. The optical band gaps were 3.22 eV, 3.20 eV, 3.37 eV and 3.35 eV for $\text{TiO}_2(\text{A})$, $\text{CuO-TiO}_2(\text{A})$, $\text{TiO}_2(\text{AB})$ and $\text{CuO/TiO}_2(\text{AB})$, respectively. Since the band gap of $\text{TiO}_2(\text{B})$ is larger than that of $\text{TiO}_2(\text{A})$, $\text{TiO}_2(\text{AB})$ as the composite of anatase TiO_2 and $\text{TiO}_2(\text{B})$ shows a higher band gap value. Similarly, the band gap values of the samples with CuO loading are lower due to the small band gap of CuO. The increase in the band gap energy probably causes a decrease in the valence band (VB) edge or an increase in the CB edge, which would lead to a decrease in the photoinduced carrier recombination rate^[19] and provide a larger driving force for the reduction of CO_2 ^[18].

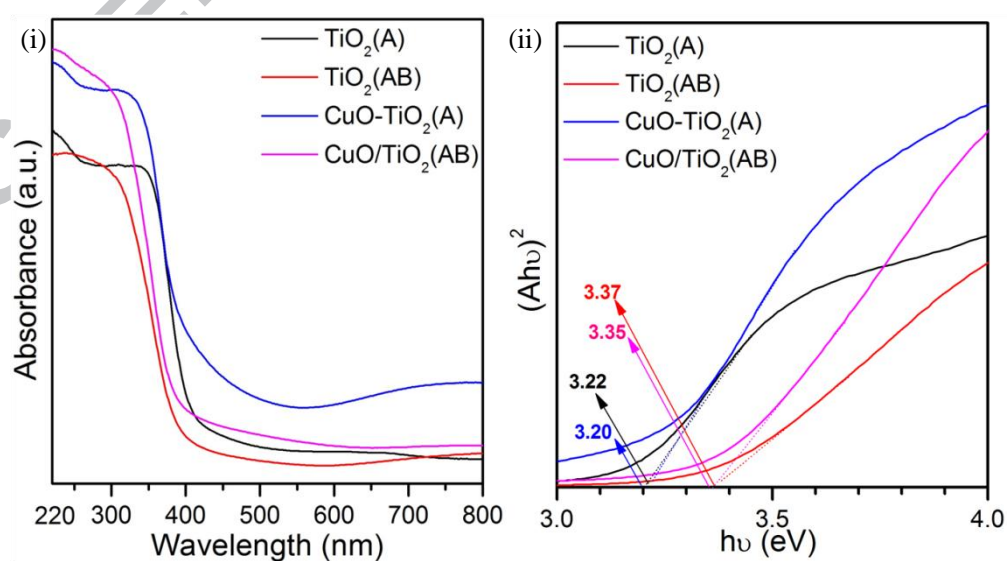


Fig. 6. (i) UV-vis diffuse reflectance spectra, (ii) plots of $(\alpha h\nu)^2$ versus the photon energy ($h\nu$) of the as-synthesized photocatalysts.

The PL spectra of all samples were obtained to determine their rate of photogenerated electron and hole recombination. Higher PL peaks indicate a higher probability of recombination, which will result in a lower photocatalytic activity^[21]. As shown in Fig. 7, the emission peak of pure anatase TiO₂ is at approximately 378 nm and exhibits the highest PL intensity. The CuO-TiO₂(A), TiO₂(AB) and CuO/TiO₂(AB) samples have emission peaks with similar intensities that are much weaker than that of TiO₂(A), which indicates that the recombination of photogenerated electrons and holes is largely inhibited. Fig. 7 clearly shows that either CuO loading or mixed-phase TiO₂ can decrease the rate of charge carrier recombination. All three of these samples can be considered composites. Their inner electric field changes, which helps to minimize/inhibit charge carrier recombination. Among all the samples, the photogenerated electrons and holes in the CuO/TiO₂(AB) composite have the longest lifetime. This confirms that a heterojunction was formed at the interface between TiO₂ and CuO. The photo-induced electrons would be shifted from the higher CB of TiO₂ to CuO, which serves as a reservoir^[16].

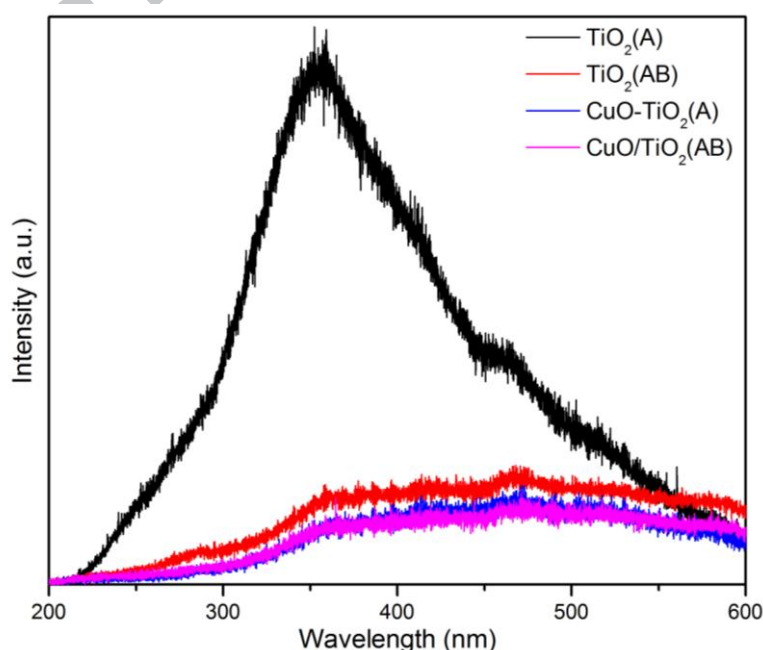


Fig. 7. PL spectra measured at room temperature for TiO₂(A), CuO-TiO₂(A), TiO₂(AB) and CuO/TiO₂(AB) photocatalysts.

The photogenerated charge transfer efficiency was evaluated by a photoelectrochemical method. As displayed in Fig. 8 i, the photocurrents of the as-prepared samples were measured during on and off cycles of irradiation. The obtained photocurrent densities decrease in the following order: $\text{CuO/TiO}_2(\text{AB}) > \text{TiO}_2(\text{AB}) > \text{CuO-TiO}_2(\text{A}) > \text{TiO}_2(\text{A})$. The rapid photoinduced e^- and h^+ separation efficiency corresponds to a high photocurrent density. Therefore, $\text{CuO/TiO}_2(\text{AB})$, a ternary hybrid structure, has a higher separation efficiency for photoinduced charge carriers under light illumination. The results of the photocurrent response versus time curves show that CuO loading or the incorporation of B phase TiO_2 into anatase TiO_2 can promote the efficient separation of photogenerated electron-hole pairs to further enhance the photocatalytic activity of $\text{TiO}_2(\text{A})$. As shown in Fig. 8 i, the photocurrent densities of $\text{TiO}_2(\text{AB})$ and $\text{CuO-TiO}_2(\text{A})$ are close and higher than that of $\text{TiO}_2(\text{A})$. $\text{CuO/TiO}_2(\text{AB})$ has the highest value. To further elucidate the separation and transfer efficiency of the photogenerated electrons and holes, the prepared catalysts were also investigated by EIS. In theory, the arc radius in the EIS Nyquist plot represents the electron transfer resistance. A smaller arc radius indicates a better migration and transfer efficiency of the photoexcited e^-h^+ pairs. The EIS (Fig. 8 ii) results are consistent with the transient photocurrent responses (Fig. 8 i). As observed in Fig. 8 ii, the arc radius of $\text{CuO/TiO}_2(\text{AB})$ is the smallest, indicating that it has the lowest charge transfer resistance on the electrode surface. A higher conductivity is conducive to the transfer of photoinduced carriers, resulting in better photocatalytic activity.

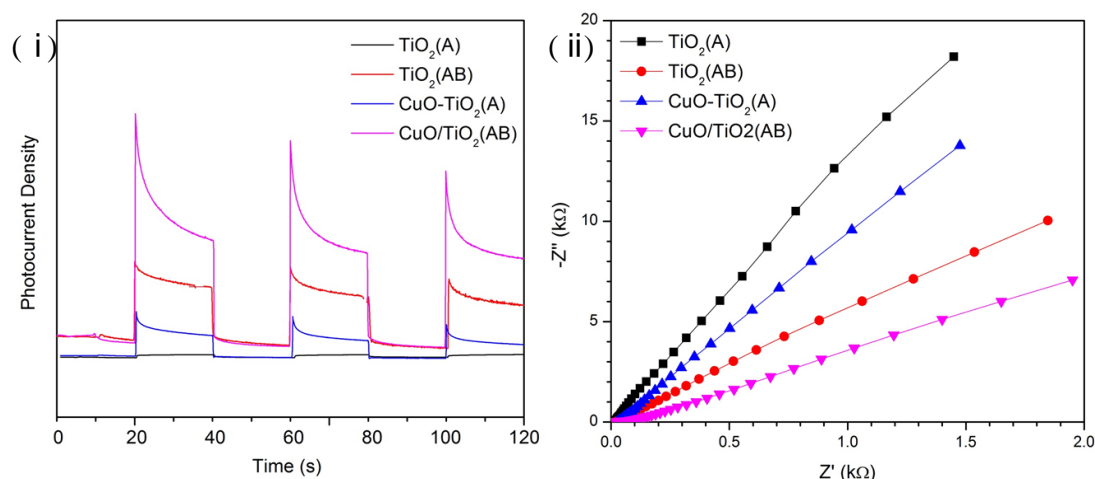


Fig. 8. (i) Photocurrent response versus time curves; (ii) EIS results of the as-prepared catalysts.

3.2. Photocatalytic CO₂ reduction performance

The photocatalytic activities of the TiO₂ and TiO₂/CuO composites were evaluated by the photoreduction of CO₂ into methyl formate (MF) in methanol. MF is an important chemical intermediate. It is a considerable and promising way to synthesize MF using clean energy under moderate conditions. Fig. 9 shows the MF yields under ultraviolet radiation for 4 h. To investigate the effect of CO₂, a contrasting experiment replacing CO₂ with N₂ in the case of CuO/TiO₂(AB) showed the MF yield slowing down from 1800 to 350 μmol•g⁻¹. This finding suggests that CO₂ made a significant contribution to the formation of MF. In Fig. 9, the MF yield clearly decreases in the following order: CuO/TiO₂(AB) > TiO₂(AB) > CuO-TiO₂(A) > TiO₂(A). The CuO/TiO₂(AB) composite possesses a higher photocatalytic activity than the other three samples for the same catalyst dosage, and this can be attributed to the effects of the mixed phases and CuO loading. The presence of two crystal phases might be equivalent to a complex of two semiconductors, promoting the effective separation of the photogenerated electrons and holes, i.e., the so-called “mixed-phase effect”. Although the UV-vis diffuse reflectance spectrum (Fig. 6 i) of TiO₂(AB) shows a blueshift compared to that of TiO₂(A), the peaks are still in a superior light intensity range for the high-pressure mercury lamp (Table S3) used here. More importantly, this

type of mixed-phase crystal is more effective in suppressing the recombination of photogenerated electrons and holes as well as transporting photogenerated carriers between two semiconductors. The above beneficial effect was largely brought by higher BET surface area of mixed-phase TiO_2 as shown in Table S1. The higher surface area is favourable for electron transport and also provides more surface reactive sites for photocatalytic CO_2 reduction process^[11,14,27]. Leaving aside surface area, formation rate of MF in unit of $\mu\text{mol}/\text{m}^2/\text{h}$ is shown in Fig.S2. The results of $\text{TiO}_2(\text{A})$ samples are superior to those of $\text{TiO}_2(\text{AB})$ samples because of lower band gap of the former with faster light response. Meanwhile, the MF yield results of the samples with CuO are better than those of the samples without CuO in Fig.S2. The presence of CuO with a low band gap leads to an increase in the full-spectrum light absorption and decreases the charge carrier recombination, allowing higher electron mobility in the composites. The synergistic effect of the above two factors (mixed phases and CuO loading) was obvious in $\text{CuO}/\text{TiO}_2(\text{AB})$, which exhibits the highest photocatalytic MF production yield of $\sim 1800 \mu\text{mol}\cdot\text{g}^{-1}$. This value is higher than that obtained with metal sulphides, as reported by Xin et al.^[29-31]. Although the MF formation rate here is somewhat lower than that obtained with $\text{Bi}_2\text{S}_3\text{-ZnIn}_2\text{S}_4$ ^[32], $\text{CdS}/\text{g-C}_3\text{N}_4$ ^[33] and CuO-TiO_2 composites^[34] with optimal formulas, the design and optimization of the component proportions of $\text{CuO}/\text{TiO}_2(\text{AB})$ will be a research priority in the future.

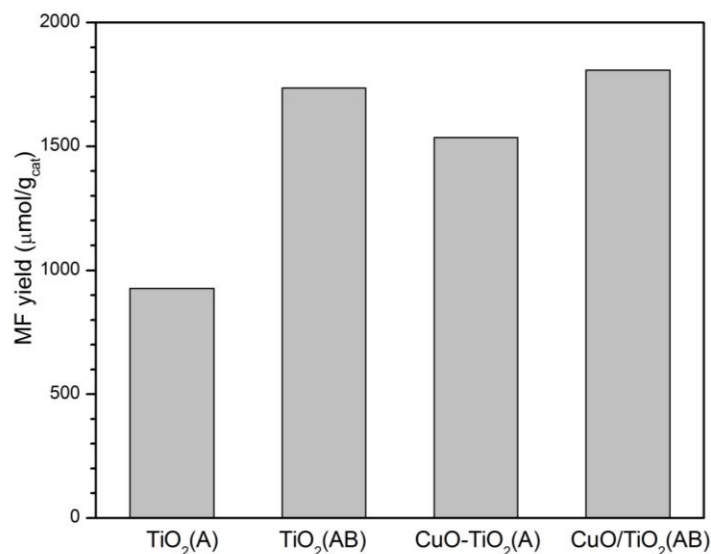


Fig. 9. The MF yields over various catalysts.

A possible mechanism for the CO₂ photoreduction to MF in CH₃OH over CuO/TiO₂(AB) catalysts under ultraviolet-light irradiation was proposed based on the above experimental results, as displayed in Fig. 10. The CB edges of anatase TiO₂, TiO₂(B) and CuO are -0.32, -0.90 and 0.46 eV, respectively, with respect to the normal hydrogen electrode (NHE), while the VB edges of anatase TiO₂, TiO₂(B) and CuO are +2.90, +2.60 and +2.16 eV, respectively [15, 18, 21]. Under UV-light irradiation, all of the anatase TiO₂, TiO₂(B) and CuO can be excited to generate photoelectrons and holes when absorbing photon energy. The electrons in the CB of TiO₂(B) are driven by the potential energy to transfer to the CB of anatase TiO₂ and then to CuO. CuO is used to trap electrons as a p-type semiconductor [12, 21, 35]. Conversely, the photogenerated hole can move from the VB of anatase TiO₂ to that of TiO₂(B) and CuO [21]. The CuO/TiO₂(AB) composite acts as a “staggered” type II heterojunction [21] system, which leads to the effective separation of the excited electrons and holes at the TiO₂(B)–TiO₂(A)–CuO interfaces. As reported, the VB potential of all components is more positive than $E_0(\text{CH}_3\text{OH}/\bullet\text{CH}_2\text{OH})$ (0.927 V) [20, 32-34], and their holes can oxidize methanol into formaldehyde with H⁺ formation. The electrons accumulate in CuO and reduce part of CuO into Cu₂O, forming Cu₂O@CuO/TiO₂(AB). The CB of Cu₂O is

more negative than $E_0(\text{CO}_2/\text{HCOOH})$ (-0.61 V)^[20, 32-34] and can reduce CO_2 into formic acid in the presence of H^+ . After donating electrons, Cu_2O oxidizes back into CuO . This is consistent with the XPS result and the experiment phenomena. The catalyst was initially an off-white color and then darkened after illumination for a while in the suspension. Eventually, the catalyst changed back to off-white after recovery. Similar explanations have been reported in the literature^[12,21]. MF can be produced through the esterification of formic acid and methanol and the dimerization of formaldehyde via the Tishchenko reaction^[32-34]. The synergistic effect of both mixed phases and CuO loading on $\text{CuO}/\text{TiO}_2(\text{AB})$ contributes to the improvement in the photocatalytic performance.

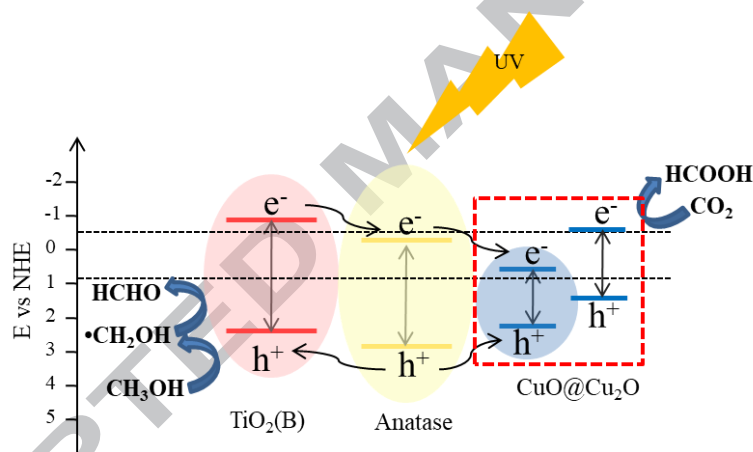


Fig. 10. Schematic of the mechanism for the CO_2 photoreduction to MF in CH_3OH over $\text{CuO}/\text{TiO}_2(\text{AB})$ catalysts.

The reusability of the photocatalysts was evaluated after recovering the catalyst from solution by centrifugation. As displayed in Fig. 11(i), the yields of MF are still above 90% under UV-light irradiation with the four recycled samples. Moreover, the two dual-phase TiO_2 microsphere photocatalysts have a better performance. When compared with those reported in the literatures^[29,30,33], the stability of our photocatalyst samples is still in an acceptable range. Time course of MF production over $\text{CuO}/\text{TiO}_2(\text{AB})$ was further investigated as shown in Fig. 11(ii), and the photocatalyst was recovered every 4 h. Continuous increases of MF amount during every round can be observed upon up to 4 h illumination. With the increase in cycle, the recyclability of

photocatalytic CO₂ reduction in methanol to MF remains above 90% of last round. CuO/TiO₂(AB) exhibits a slightly decrease in photocatalytic CO₂ reduction performance. In addition, XRD and SEM analyses were carried out on the CuO/TiO₂(AB) catalysts after the first cycle of photoreduction, as displayed in Fig. S3. The XRD results show that all the diffraction peaks of the CuO/TiO₂(AB) composites are basically the same before and after the photocatalytic reaction. Only the intensity of the peak at 25.3° in the XRD pattern of CuO/TiO₂(AB) after use decreases, as shown in Fig. S3. In the recovery operations, the structure or components of the catalyst samples might be affected. The highly dispersed microsphere morphology did not change, as shown in the SEM image, after the photocatalytic CO₂ reduction reaction. All of the above results demonstrate relatively good stability of CuO/TiO₂(AB) during the photocatalytic reaction processes. In the future, optimization of the recovery operations will be another research point for further improving the stability of the photocatalysts in cyclic runs.

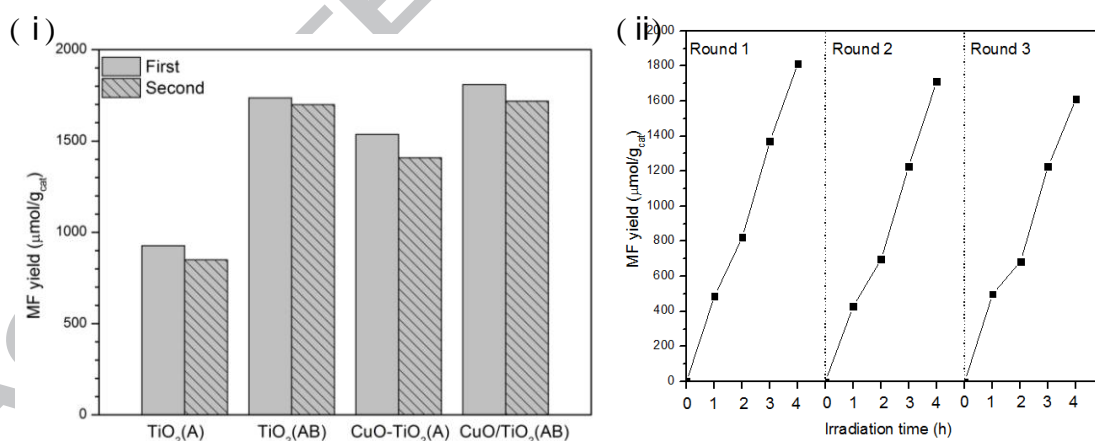


Fig. 11. (i) Reusability of the as-prepared catalysts for photocatalytic CO₂ reduction in methanol; (ii) Time dependence of MF yield over CuO/TiO₂(AB) in three cyclic runs.

4. Conclusions

CuO-decorated anatase and B dual-phase TiO₂ microsphere (CuO/TiO₂(AB)) photocatalysts were synthesized using a facile two-step method and used for the photoreduction of CO₂ in methanol. The structural and chemical composition analyses confirmed the existence of

mixed-phase TiO₂ with highly dispersed CuO on the surface. Compared with anatase TiO₂, CuO-loaded anatase and dual-phase TiO₂ without CuO, CuO/TiO₂(AB) had the highest photocatalytic MF production yield and can be considered a mixed-phase heterojunction composite. The synergistic effect of both mixed phases and CuO loading contributed to the high photocatalytic activity, which was a result of the enhanced light response to UV light, and effective separation and reduced recombination of photoinduced charge carriers. CuO/TiO₂(AB) also showed good reusability and stability during the photocatalytic reaction process.

Conflicts of interest

There are no conflicts of interest to declare.

Acknowledgements

This work was supported by the National Natural Science Foundation of China (51802160 and 51808296), the Natural Science Foundation of Jiangsu Province of China (BK20150892 and BK20170938), the Natural Science Foundation of Jiangsu Higher Education Institution of China (15KJB610012), and the 63rd Chinese Postdoctoral Science Foundation (2018M630487). Dr. Y. Zhao and Dr. Wei Cai are grateful for the Startup Foundation for Introducing Talent of NUIST (S8113082001 and 2243141601034). In addition, Wei Cai would also like to acknowledge support and helpful discussion from the WECHAT group named “Energetic and Progressive Mightyboy”!

Supporting Information

Supplementary material associated with this article can be found in the online version.

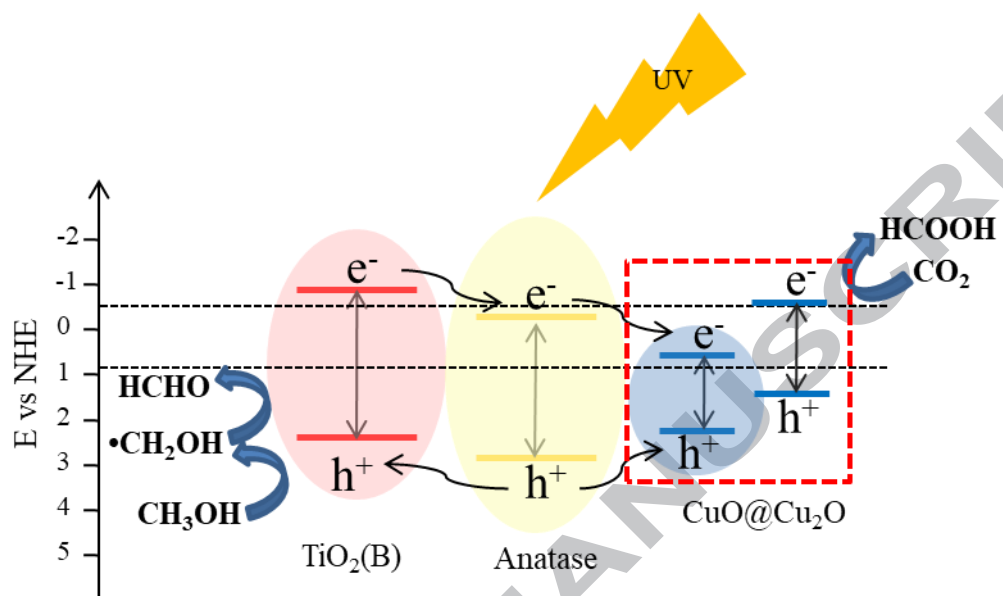
References

[1] A. Fujishima, K. Honda. *Nature*, 5358, (1972)37.

- [2] B. Dong, T. Liu, C. Li, et al. *Chinese Chem. Lett.*, 5(2018) 671.
- [3] S.Y. Lee, S.J. Park. *J. Int. Eng. Chem.* 6(2013) 1761.
- [4] Z. Xiong, H. Wang, N. Xu, et al. *Int. J. Hydrogen. Energ.* 32 (2015)10049.
- [5] K. Qi, B. Cheng, J. Yu, et al. *Chinese J. Catal.* 12(2017) 1936.
- [6] Z. Jiang, X. Zhang, Z. Yuan, et al. *Chem. Eng. J.* 348(2018) 592.
- [7] M. Li, M. Wang, L. Zhu, et al. *Appl. Catal. B-Environ.* 231(2018) 269.
- [8] Y. Zhao, Y. Wei, X. Wu, et al. *Appl. Catal. B-Environ.* 226(2018) 360.
- [9] B. Li, Y. Hao, B. Zhang, et al. *Appl. Catal. A-Gen.* 531(2017) 1.
- [10] P. Chaudhari, S. Mishra. *Measurement.* 90(2016)468.
- [11] I. H. Chowdhury, S. Ghosh, S. Basak, et al. *J. Phys. Chem. Solids.*104(2017) 103.
- [12] Y. T. Liao, Y. Y. Huang, H. M. Chen, et al. *ACS Appl. Mater. Inter.* 49(2017) 42425.
- [13] M. Gao, S. W. L. Ng, L. Chen, et al. *J. Mater. Chem. A.* 22(2017) 10909.
- [14] A. Taufik, A. Albert, R. Saleh. *J. Photoch. Photobio. A-Chem.* 344(2017) 149.
- [15] M. H. Razali, M. Yusoff. *Mater. Lett.* 221(2018) 168.
- [16] M. K. Hossain, A. R. Koirala, U. S. Akhtar, et al. *Chem. Mater.* 27(2015) 6550.
- [17] T. Di, J. Zhang, B. Cheng, et al. *Sci. China Chem.* 3(2018) 344.
- [18] J. Si, Y. Wang, X. Xia, et al. *J. Power Sources*, 360(2017) 353.
- [19] P. Periyat, K. V. Baiju, P. Mukundan, et al. *Appl. Catal. A: Gen.*, 349(2008) 13-19.
- [20] S. Qin. *Photoreduction of CO₂ in methanol to prepare methyl formate using CuO-TiO₂.*
Tianjin University, 2010.
- [21] M. Golestanbagh, M. Parvini, A. Pendashteh. *Catal. Lett.* 148 (2018) 2162.
- [22] C. Wang, X. Zhang, Y. Liu. *Nanoscale.* 10(2014) 5329.

- [23] W. Cai, B. Yu, Y. Zhao, et al. Chem. Eng. J. 317(2017) 376.
- [24] W. Cai, Y. Zhao, M. Chen, et al. Chem. Eng. J. 333(2018) 414.
- [25] M. Edelmannová, K. Y. Lin, J. C. S. Wu, et al. Appl. Surf. Sci. 454(2018) 313.
- [26] Z. Q. Li, L. Mo, W. Chen, et al. ACS Appl. Mater. Interfaces, 9(2017) 32026.
- [27] J. Zheng, L. Mo, W. Chen, et al. Nano Research, 10(2017) 3671.
- [28] J. Dong, J. Ye, D. Ariyanti, et al. Chemosphere. 204(2018) 193.
- [29] J. Chen, F. Xin, S. Qin, et al. Chem. Eng. J., 230(2013) 506.
- [30] J. Chen, S. Qin, G. Song, et al. Dalton T. 42(2013) 15133.
- [31] J. Chen, F. Xin, X. Yin, et al. RSC Adv. 5(2015) 3833.
- [32] J. Chen, F. Xin, H. Niu, et al. Mater. Lett. 198(2017) 1.
- [33] X. Yang, W. Xin, X. Yin, et al. Chem. Phys. Lett. 651(2016) 127.
- [34] S. Qin, F. Xin, Y. Liu, et al. J. Colloid Interf. Sci. 1(2011) 257.
- [35] K. K. Mandari, J. Y. Do, S. V. P. Vattikuti, et al. J. Alloy. Compd. 750 (2018) 292.

Graphical Abstract



Highlights

1. CuO-decorated anatase and B dual-phase TiO₂ microsphere (CuO/TiO₂(AB)) photocatalysts were successfully synthesized.
2. CuO/TiO₂(AB) photocatalysts exhibited high catalytic activity for CO₂ reduction to HCOOCH₃ in CH₃OH solution.
3. CuO/TiO₂(AB) can efficiently enhance the photogenerated charge separation.
4. CuO/TiO₂(AB) acted as a mixed-phase heterojunction composite.